Acta Geophysica
https://doi.org/10.1007/s11600-023-01165-7

RESEARCH ARTICLE - SOLID EARTH SCIENCES

Seismo ionospheric anomalies related to the M_w 7.5, Kepulauan Alor, Indonesia earthquake

Kevser Koklu[1]

Received: 11 April 2023 / Accepted: 8 July 2023
© The Author(s) under exclusive licence to Institute of Geophysics, Polish Academy of Sciences & Polish Academy of Sciences 2023

Abstract
Discussions about anomaly in the ionosphere have made significant progress since the great Alaskan earthquake, in 1964. Specifying signs of precursors of an earthquake and traces of the aftershock of its may minimize every kind losses. This study examines the possible effect on the ionosphere of the M7.5 earthquake that occurred at 21:46 UT on November 11, 2004, near Kepulauan, Alor Islands (8,152°S–124,868°E), Indonesia. This effect is observed in TEC (TECU) data. The limits of the TEC data gained from IRI-2016 are determined by the statistical method. Anomalies are marked by means of out-of-bounds data. Anomaly causes are introduced to the reader according to the principle of causality. In this context, a portrait of space climate conditions is drawn with the aid of the earthquake, geomagnetic storm, and solar activity effect. According to this portrait, we perceive on October 15, November 10, and December 1–11. Probably the November 10 anomaly is caused by the earthquake and the other anomaly days may be related to the aftershock of the earthquake.

Keywords November, 2004, Kepulauan Alor · Earthquake · Total electron content (TEC) · Geomagnetic storm (GS) · Solar activity (SA)

Introduction

The earthquake (EQ), which exists in the dynamic life cycle of nature, still possesses its unknown. Relatively unpredictable EQ event causes great regional destruction in the life of living, location of settlements, and ecosystems. There is a need to develop both short and long timescale EQ prediction techniques in order to reduce the losses and the post-event destructive effect to some extent. The EQ prediction from the past to the present gives wide opportunities to study researchers. The relationship between seismic events and ionospheric activity is now more clearly stated.

The ionosphere lies up the atmosphere at an above of 50 to 1100 km, where there is a significant amount of ions and free electrons that allow the movement of electromagnetic waves. Most of the gases in the ionosphere are neutral. They are commonly shaped as a product of the ionization of wave emissions from the Sun. The sum of unrestricted electrons in this layer is related to various reasons such as time, location, temperature, and geomagnetism. This layer, daily for 27 days, exhibits regular 6-month, seasonal, and 11-year changes seasonally. Almost all of the effects of these modelable changes can be specified. Besides consistent changes, the source of unexpected variations is geomagnetic storms (GSs) (Fu et al. 2013, 2017; Paul et al. 2019, 2020; Eroglu 2018, 2019, 2020; Koklu 2020, 2021, 2022; Dayanandan et al. 2020; Inyurt 2020; Basciftci 2021, 2022, 2023), space weather conditions (Bilitza 2001; Bagiya et al. 2009; Olwendo et al. 2012; Inyurt et al. 2017; Patari et al. 2021; Eroglu 2022a, b, c; Konakoglu et al. 2023; Baral et al. 2023), solar activity (SA) (Inyurt and Razin 2021), EQ–crust movements (Igarashi et al. 1995; Freund et al. 2009; Yildirim et al. 2016; Ke et al. 2018; Senturk et al. 2020; Tariq et al. 2019; Inyurt et al. 2017; Yasuoka et al. 2005; Kim et al. 2018; Eroglu 2022a, b, c, 2023), volcanoes (Dautermann et al. 2009), and anthropogenic impact (Lin et al. 2017).

In order to counteract the devastating effects of an EQ, the tracking of precursor signs is vital for modeling and forecasting. The signals can be considered by means of the causality principle (Eroglu et al. 2012; Isik et al. 2014).

Edited by Dr. Nikolay Palshin (ASSOCIATE EDITOR) / Prof. Ramon Zuñiga (CO-EDITOR-IN-CHIEF).

✉ Kevser Koklu
ozkoklu@yildiz.edu.tr; kevserkoklu@gmail.com

[1] Department of Mathematical Engineering, Yildiz Technical University, Davutpasa Campus, Istanbul 34220, Turkey

Published online: 30 August 2023

The movement of the earth, besides being the result of the break in the fault line, is also caused by changes that human beings cannot perceive directly. One of the keys to examining these changes or abnormal situations is the total electron content (TEC). TEC (TECU), which is one of the essential tools of the ionosphere and signs the whole quantity of free electrons, is specified as the total amount of electrons in a 1 m^2 topological shape. 1 TECU is considered to be about 10^{16} electrons/m^2 (Schaer 1999). EQ–ionosphere relationship studies start with the big Alaskan EQ (Davies and Baker 1965) and reveal that tectonic events may also source ionospheric anomalies. Researchers exhibit different approaches for the recognition of TEC anomalies related to the EQ. Anomalies can be classified as negative or positive on a given day. When an anomaly signs higher than the TEC data's higher confidence bound, then it is called a positive anomaly. When an anomaly signs inferior than the lower confidence bound, it is called a negative anomaly. Regular or irregular ionospheric fluctuations can be triggered by different reasons such as GS, SA, and geomagnetic field oscillations. Consequently, researchers should separate different anomaly effects for predicting EQs. One may compare some selected TEC anomaly's paper such as 1 day (Politis et al. 2022), 3 days (Khan et al. 2022; Yildirim et al. 2016), 5 days (Shah et al. 2022; Eroglu et al. 2023), 6 days (Eroglu 2022a, b, c), 8–9 days Senturk et al. 2020), and 10 days (Tariq et al. 2019).

This work investigates the likely impacts of the EQ (M_w 7.5) that occurred near Kepulauan Alor (8.152°S – 124.868°E) in Indonesia at 21:46 UT on November 11, 2004. For this purpose, first of all, 61-day solar wind parameters such as the (Bz (nT) magnetic field, the E (mV/m) electric field, the solar wind speed v (km/s), the dynamic pressure P (nPa), the proton density N ($1/cm^3$)), zonal geomagnetic indices (Dst (nT) and Kp (nT)), and F10.7 (sfu) index values with SA effect are examined. Secondly, IRI-2016 TEC values are obtained according to the latitude and longitude of the epicenter of the EQ by using the International Reference Ionosphere (IRI). Finally, TEC anomaly limits are considered from the TEC map. The study begins by detecting the literature. Then, with the Fourier transformation, the TEC map in the time–space is converted to the frequency–space and anomaly reading is constructed over the amplitudes. The compatibility of the results obtained with the Fourier spectral analysis with the anomaly values is remarkable. Following this analysis, the limits (boundaries) of the TEC are determined. Anomalies are detected under the guidance of these limits. Careful examination of the anomaly causes is possible by discussing space weather conditions, GSs, SA, and EQ effects.

In the study, 15 October and 10 November anomalies are determined before and 2–11 December anomalies after the EQ. The closest ionospheric anomaly to the 11 November Alor EQ date belongs 1 day ago.

Method and material

The place of the event

On November 11, 2004, at 21:46 UT, Indonesia was faced with a massive Mw 7.5 EQ with a depth of 10, lasting 38 s, near Kepulauan Alor (8,152°S–124.868°E). The Alor EQ occurs as a consequence of narrow faults on or neighboring the border between the Banda Sea microplate in the north and the Timor microplate in the south. Focal instrument resolutions show that the break happened either on a steep,

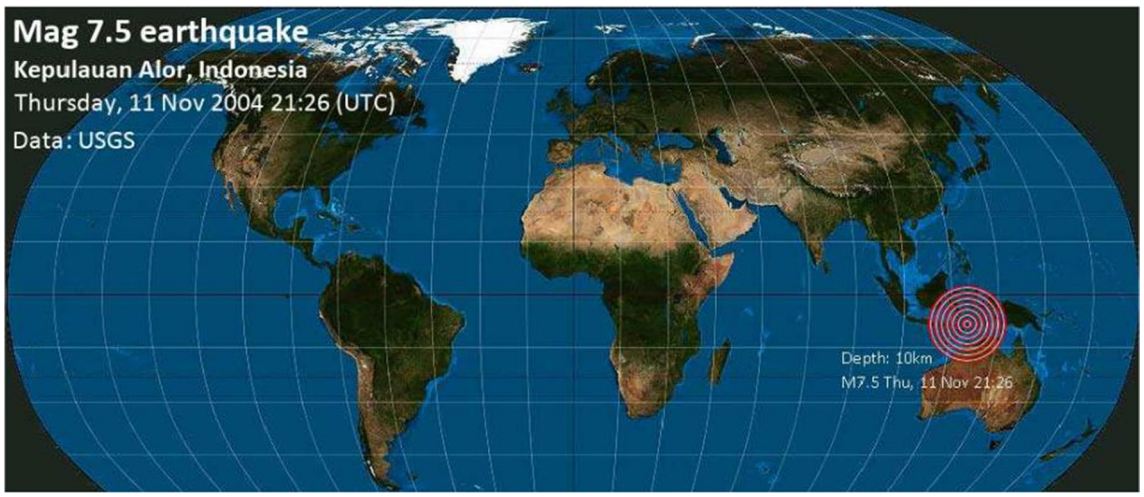

Fig. 1 EQ location and epicenter

vertical contrary fault line or on a shallow, south-sloping thrust fault. The EQ place atlas is shown in Fig. 1.

The TEC data

In our paper, the TEC data gained from the IRI (2016) are used according to the latitude and longitude of the EQ epicenter. The IRI model is a model produced by the association of the URSI and the COSPAR and is regularly improved and developed. The latest form of the model with online data is the IRI-2016 map. According to the given location, date, and time, IRI is able to run a number of parameters associated with the ionosphere, together with the TEC data for ionosphere altitudes between 50 and 2000 km. The main map bases of the IRI model are radar, international satellites for ionosphere studies, and Alouette receivers. The TEC values can be calculated online at the internet address (https://ccmc.gsfc.nasa.gov/modelweb/models/iri2016_vitmo.php) with the aid of the IRI-2016 program.

The Fourier transform

Equation (1) displays the time-dependent function "t" to the frequency-dependent function "w." This operation's name is Fourier transform that uses the TEC map for spectral analysis (Debnath and Bahatta 2007; Koklu 2018; Ozden Koklu 2018). The Fourier transform:

$$\mathcal{F}\{f(t)\} = \int_{-\infty}^{\infty} e^{-iv2\pi t} f(t)\mathrm{d}t, \tag{1}$$

where the angular frequency is $\omega = 2\pi v$, time is t, and the cycle frequency per second is v. Equation (1), the Fourier integral, proposes that the time-domain $f(t)$ signal with the transformation can be equivalent to its spectrum. The Fourier transform is a mathematical method that is used to decompose a signal into its constituent frequencies. It is widely used in various fields including engineering, physics, mathematics, and signal processing. The Fourier transformation transforms from the time-domain function to the frequency-domain function. This means that unobservable in the time-domain amplitudes can be easily observed in the frequency period. The Fourier transform can be used to identify the frequencies present in a signal, as well as the amplitude and phase of each frequency component. The work employs the spectral analysis of the TEC data *short-term* Fourier transformation (STFT). In this way, one may realize ionospheric anomalies in the frequency domain. Figure 2 shows the STFT of the TEC data by displaying frequency.

In the light of frequency period amplitudes (Fig. 2), the abnormality is observed in the amplitudes between October 12 and 20, October 21 and 23, October 26 and 27, and November 2 and 11. The ionospheric anomalies overlap the amplitudes.

Statistical method

Limits define the framework of the statistical method. The lower limit and upper limit are indicated by the median ± 1.34*standard deviation (σ) respectively (Klotz and Johnson 1983). If the TEC map shows rates fewer than the lower limit or more than the upper limit for separately hour, it is noticed as an anomaly. The lower limit and upper limit are determined by using the 61-day TEC values obtained from IRI-2016. Statistical limits:

$$\text{Lower Limit} = \text{Median} - 1.34\sigma, \tag{2}$$

$$\text{Upper Limit} = \text{Median} + 1.34\sigma. \tag{3}$$

If TEC data are specified below the lower limit, it is noticed as a negative anomaly, if it is observed above the upper limit, it is noticed as a positive anomaly. Table 1 exhibits the anomalies that are shown together with their days and hours obtained from Eqs. (2) and (3). In Table 1, A- indicates a negative anomaly, and A + indicates a positive anomaly. In determining of anomaly day, the lower and the upper boundaries are observed from thirty-one day.

13-day anomalies (two days are at the pre-EQ) are monitored for the TEC map. As stated in Table 1, the specified anomalies are on October 15, November 10 (the day before the EQ), December 1–11 between (thirteen days). The statistical method rates approve to the STFT frequencies (Fig. 2).

Results and discussions

The physical background of the TEC anomaly

The ionosphere is a coating of the atmosphere that is ionized by planetary radiation. It is meaningful for radio signals, as it reflects radio waves back to the Earth's surface. The TEC is a measure of the total amount of electrons in a column of the ionosphere above a particular location. TEC anomalies refer to deviations from the expected TEC values. Ionospheric anomalies (Davies and Baker 1965; Freund et al. 2009; Ke et al. 2018; 2020; Bulbul and Basciftci 2021; Basciftci and Bulbul 2022, 2023; Eroglu 2022a, b; Patari et al. 2021; Satti et al. 2022; Shah et al. b, c; Politis et al. 2022; Khan et al. 2022; Baral et al. 2023) can occur due to a variety of factors, including GSs, SAs, solar flares, EQs, volcanic effects, anthropogenic effects, and ionospheric irregularities. GSs, SAs, and EQs are reasoned by disturbances in the Earth's magnetic field, which can

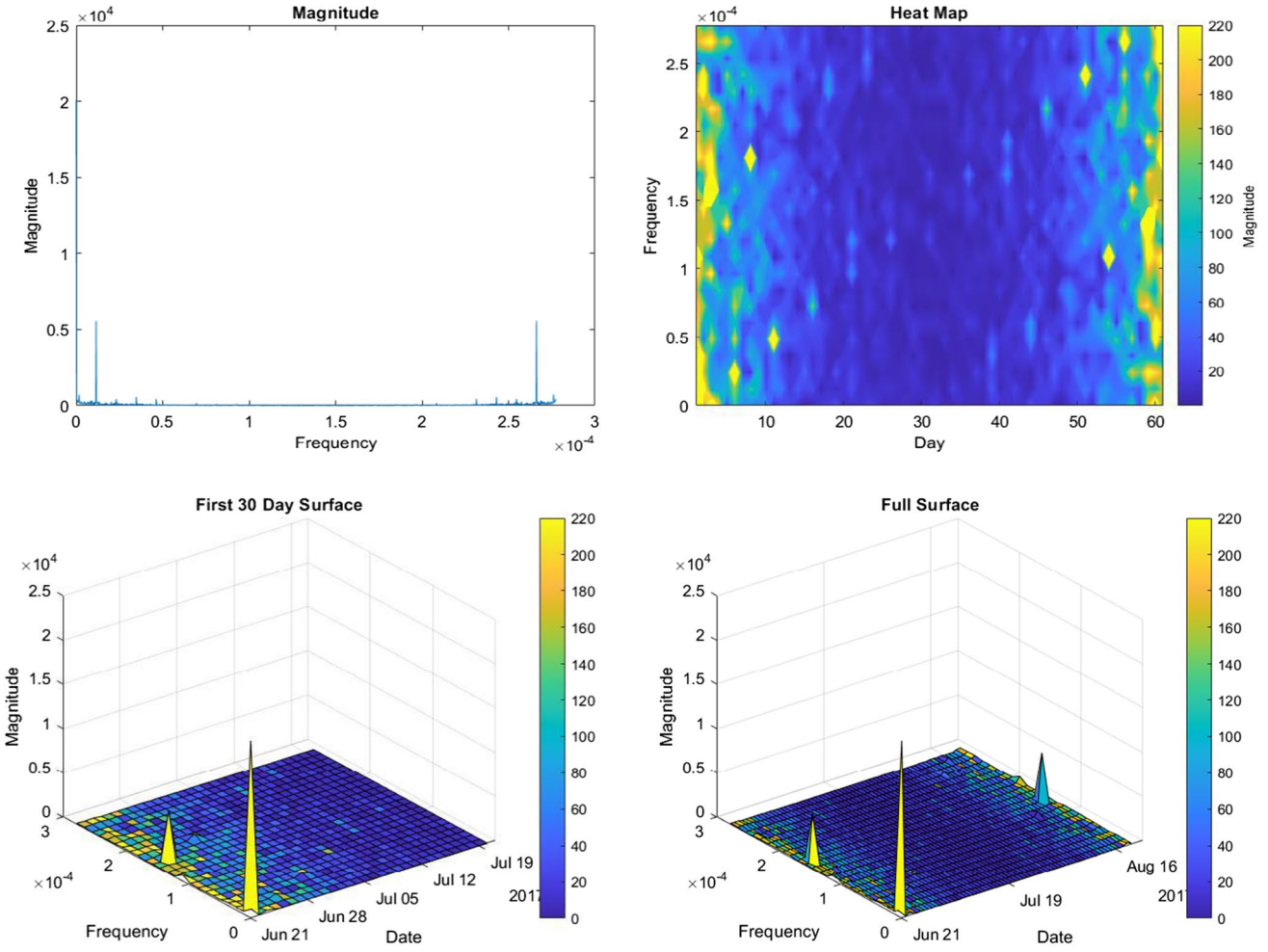

Fig. 2 STFT appearance

cause changes in the ionosphere. Solar flares are bursts of energy from the Sun that can also impact the ionosphere. EQs, due to the high energy they possess and release, likely affect the ionosphere TEC cross section from the Earth's crust through energy-dense particles containing heat and gas. Ionospheric irregularities refer to generally small-scale variations in the ionosphere, which can cause localized TEC anomalies. Therefore, determining the reason for anomalies is critical for the prediction of natural events that leave heavy traces such as EQs. The fact that there is still no consensus in the discussions in this area means that anomaly studies should continue persistently. TEC anomalies may have impacts on radio signals, navigation, and satellite operations. TEC anomalies can cause signal attenuation, phase delay, and scintillation, which can degrade the performance of GPS and other satellite-based navigation systems. Therefore, understanding TEC anomalies is important for improving the accuracy and reliability of these systems.

To study TEC anomalies, one typically uses data from ground-based GPS receivers and satellite-based GPS receivers. By analyzing the TEC data from these sources, one can identify and characterize TEC anomalies and understand their underlying causes.

This work investigates GS effect by the aid of the solar wind parameters, and zonal geomagnetic index (the B_z (nT) *magnetic field*, the E (mV/m) *electric field*, the *solar wind speed* v (km/s), the *dynamic pressure* P (nPa), and the *proton density* N ($1/cm^3$)) and the *zonal geomagnetic indices* (Dst (nT) and Kp (nT)) examine SA effect by the aid of the F10.7 (sfu) index. The data are collected from OMNI web.

Observing the space climate condition for 61 days is crucial for the detection of the anomaly. Nine GSs, which are four of them pre-EQ, are realized on all days of the anomaly detection. The sixty-one days (61*24 = 1464-h) oscillation of the variables is perceived in Fig. 3. The red line is the EQ day that is located in the mid.

GSs (Tsurutani et al. 2006) are a type of space weather phenomenon that can have consequential impacts on

Table 1 Anomaly days of the Alor EQ discussion

Hour (UT)	October 15	November 10	December 1	December 2	December 3	December 4	December 5	December 6	December 7	December 8	December 9	December 10	December 11
00:00			A−	A−	A−	A−	A−	A−	A−	A−	A−	A−	A−
01:00				A−	A−	A−	A−	A−	A−	A−	A−	A−	A−
02:00				A−	A−	A−	A−	A−	A−	A−	A−	A−	A−
03:00	A+			A−	A−	A−	A−	A−	A−	A−	A−	A−	A−
04:00	A+	A+		A−	A−	A−	A−	A−	A−	A−	A−	A−	A−
05:00	A+	A+		A−	A−	A−	A−	A−	A−	A−	A−	A−	A−
06:00	A+			A−	A−	A−	A−	A−	A−	A−	A−	A−	A−
07:00	A+	A+		A−	A−	A−	A−	A−	A−	A−	A−	A−	A−
08:00	A−	A−		A−	A−	A−	A−	A−	A−	A−	A−	A−	A−
09:00	A−			A−	A−	A−	A−	A−	A−	A−	A−	A−	A−
10:00	A−			A−	A−	A−	A−	A−	A−	A−	A−	A−	A−
11:00			A−	A−	A−	A−	A−	A−	A−	A−	A−	A−	A−
12:00			A−	A−	A−	A−	A−	A−	A−	A−	A−	A−	A−
13:00				A−	A−	A−	A−	A−	A−	A−	A−	A−	A−
14:00			A−	A−	A−	A−	A−	A−	A−	A−	A−	A−	A−
15:00			A−	A−	A−	A−	A−	A−	A−	A−	A−	A−	A−
16:00		A−	A−	A−	A−	A−	A−	A−	A−	A−	A−	A−	A−
17:00			A−		A−	A−	A−	A−	A−	A−	A−	A−	A−
18:00	A−									A−	A−	A−	A−
19:00			A−	A−	A−	A−	A−	A−	A−	A−	A−	A−	A−
20:00		A−	A−	A−	A−	A−	A−	A−	A−	A−	A−	A−	A−
21:00		A−	A−	A−	A−	A−	A−	A−	A−	A−	A−	A−	A−
22:00		A−	A−	A−	A−	A−	A−	A−	A−	A−	A−	A−	A−
23:00		A−	A−	A−	A−	A−	A−	A−	A−	A−	A−	A−	A−

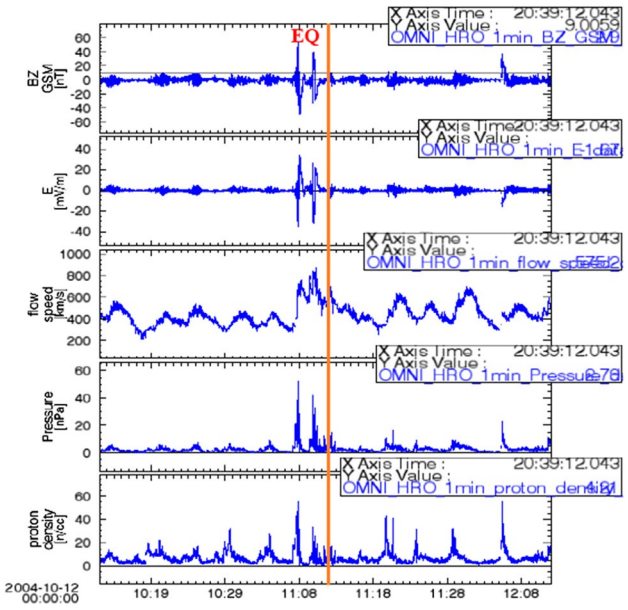

Fig. 3 B_z (nT) magnetic field, the E (mV/m) electric field, the v (km/s) solar wind speed, the P (nPa) dynamic pressure, and the N (1/cm^3) proton density appearance

Earth's magnetic field and ionosphere. GSs are caused by disturbances in the planetary wind, which is a stream of charged energetic units that bursts from the Sun. When the solar wind encounters Earth's magnetic field, it can trigger fluctuations and disturbances that result in a GS. A storm begins (sudden commencement) with a momentary ejection from the sun, called a coronal mass ejection (CME). CMEs are huge explosions of energy-dense plasma and magnetic fields from the Sun's corona. They are often associated with solar flares and can have a significant impact on Earth's space environment, including the planet's magnetic field and atmosphere. CMEs are caused by the release of magnetic energy stored in the Sun's corona. When the magnetic field lines of opposite polarity in the corona interact and reorganize, they can trigger a CME. CMEs potentially contain billions of tons of plasma and magnetic fields and can reach very high speeds. They are often described as bubble-shaped, with the plasma and magnetic field forming a structure called a magnetic flux rope. CMEs have a significant impact on Earth's space environment, including creating GSs, disrupting satellite communications, and affecting power grids. They can also produce auroras and enhance the radiation environment in space. Sudden peaks in the P (nPa) dynamic pressure and the N (1/cm^3) proton density are observed after relative decreases in the v (km/s) solar wind speed. Unexpectedly, the dynamic pressure exhibits an acceleration. At the same time, the proton density also jumps. This bursting or scattering is CME. In a sense, it is the commencement of the storm. This procedure is followed by the main phase of the GS. After the first CME, the B_z (nT) component of the magnetic field directs from the northward to the southward. During this orientation, positive magnetic field values are replaced by negative values. The Dst (nT) index also points to its minimum rate, usually a few hours after the B_z (nT) magnetic field sees its negative deep. This phase is the main phase of the GS. This phase is followed by the recovery phase. Parametric values, which fluctuate throughout the GS, try to calm down. The storm, which starts with a sudden commencement, ends with the recovery phase after passing the main phase. In the main phase, the Dst (nT) index takes its minimum value after the Bz (nT) magnetic field shows its negative minimum value. In the recovery phase, storm parameters return to pre-storm scores.

Figure 3 displays oscillation of the variables over the 61 days.

The Bz (nT) field fluctuates throughout the 61-day event period, October 13–15, October 19–25, October 29—November 10, November 16–17, November 20–22, November 28–30, and December 5–11. The Bz field

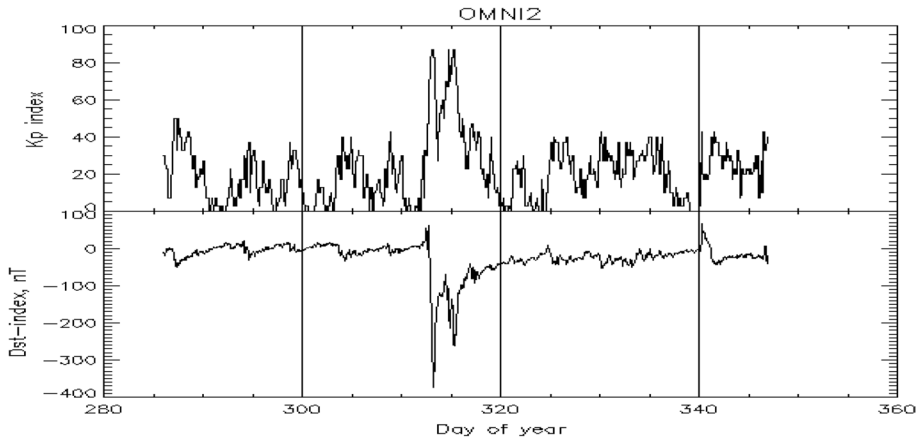

Fig. 4 Kp (nT) and Dst (nT) fluctuations

reaches its lowest rate at -44.9 nT at 03:00 UT on November 8 superstorm (Fig. 4).

The dynamic pressure P (nPa) is generally stable throughout the process. It fluctuates between November 7 and 12 and December 5 and 6. Before the superstorm, it appears before the reader with a rather unstable attitude. It shows a very high value of 39.89 nPa at 19:00 UT on November 7.

Solar wind speed (v km/s) fluctuates throughout the 61-day period. It hits extremum values of 824 km/s and 295 km/s rates. On November 9, at 22:00 UT it shows a maximum rate of 824 km/s, and the smallest rate of 295 km/s on October 17, at 03:00 UT on December 5, and at 04:00 UT.

It would be appropriate to detail the November 8 superstorm. This superstorm is an enormously powerful event with a Dst $= -374$ nT score. The first CME of this event is observed at 15:00 UT on November 6. In the first CME, the dynamic pressure revs from 1.11 nPa to 5.31 nPa, and the proton density accelerates from 5.3 to 18.2 1/cm^3. These revs are the precursor of a very powerful natural event. Then the second relatively weaker CME is observed around 02:00 UT on November 7. The dynamic pressure jumps from 0.95 nPa to 2.92 nPa and the proton density jumps from 4.7 to 11.0 1/cm^3. The third instantaneous explosion is observed at 10:00 UT on the same day. The dynamic pressure suddenly accelerates from 4.77 to 15.05 nPa, while the proton density accelerates from 23.3 to 51.2 1/cm^3. Then, at 06:00 UT on November 8, the superstorm hits. If the storm period is considered to be 5 days (120 h), in this period, the B_z component of the magnetic field hits its minimum value of -44.9 nT at 03:00 UT on November 8 during the process. The dynamic pressure, on the other hand, indicates its maximum value of 39.89 nPa on 7 November at 19:00 UT. The proton density, on the other hand, indicates its maximum value of 84.9 1/cm^3 at 12:00 UT on November 7.

GSs can be classified by the help of the Dst (nT) index as weak, moderate, severe, and super. Table 2 displays GSs related to the 61-day EQ problem period.

The "first CME" from Table 2 marks the CME through the P (nPa) and the N (1/cm^3). The "first" indicates the primary CME, and the "to" displays after one hour rate. The "time" shows the minimum rate time of the Dst index. The B_z and Dst minimum rates in Table 2 indicate the minimums of the GS.

The prompt penetration electric field (PPEF) is an essential concept in the field of atmospheric electricity, which is concerned with the study of electrical phenomena that occur in the Earth's atmosphere. PPEFs (http://www.geomag.us/models/PPEFM/RealtimeEF.html) refer to the electric field generated in the lower ionosphere during a discharge. This electric field is responsible for the propagation of the discharge through the atmosphere. For interpreting the changing of the solar wind, it is suitable to monitor the PPEFs. They are the prompt reply of the local equatorial electric field to the solar wind oscillation (Manoj et al. 2008; Tsurutani et al. 2008). The prompt penetration electric field is generated by the rapid discharge of electrical energy. This discharge generates a large current that produces a magnetic field, generating an electric field. This electric field can penetrate the lower ionosphere, which is the region of the atmosphere that extends from up to 80 km above the Earth's surface. The green alternation of the PPEFs in Fig. 5 is the *penetration* part, and the violet one is the *quiet* part. The violet part of the real-time electric field (Fig. 5) relates to the 81-day mean of the F10.7 (sfu) SA index (Manoj and Maus 2012). The article utilizes 27° E longitude, which fits to the EQ epicenter, and Fig. 5 exhibits October 13–17, November 10, 27–29, and December 1–11.

During fluctuation of the solar wind, PPEFs react punctually (Tsurutani et al. 2008). With GSs, PPEFs reason fluctuation and ionospheric anomalies (Tsurutani et al. 2008; Mannucci et al. 2009). One may see magnetic situation from

Table 2 Geomagnetic storms

Date		CME First CME				Geomagnetic Storm		
Day of Year	GS Time (UT)	P (nPa) first	P (nPa) to	N (1/cm^3) first	N (1/cm^3) to	B_z (nT) min	Dst (nT) min	Type
287	08:00	1.31	2.07	4.3	5.8	−8.6	−49	Weak
294	15:00	2.06	2.62	10.5	12.8	−7.2	−32	Weak
304	09:00	2.11	2.68	10.7	13.5	−6.3	−33	Weak
313	06:00	1.11	5.31	5.3	18.2	−44.9	−374	Super
325	19:00	2.52	3.30	11.3	14.9	−7.4	−44	Weak
330	04:00	1.61	2.72	4.8	7.9	−6.4	−53	Moderate
333	06:00	1.31	1.57	4.4	5.0	−5.5	−50	Moderate
342	02:00	1.07	4.0	6.2	18.8	−8.8	−44	Weak
346	21:00	1.88	2.98	6.1	10.1	−7.1	−41	Weak

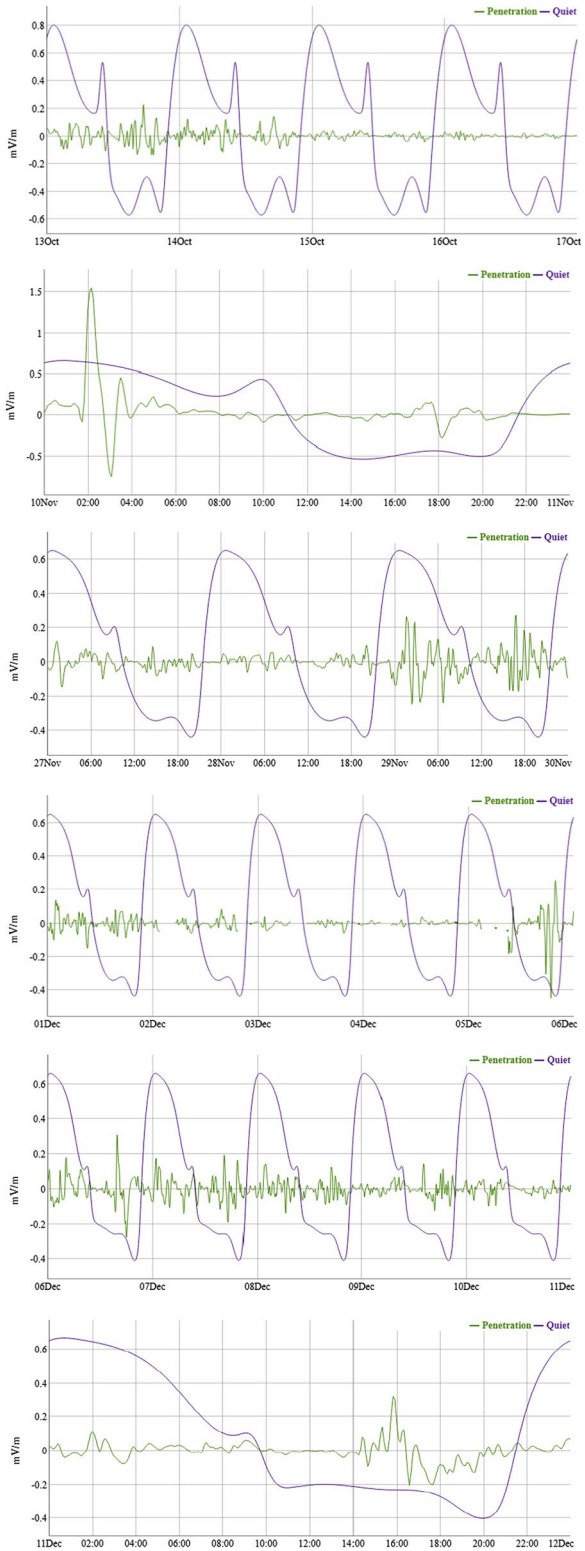

Fig. 5 PPEFs at 27°E longitude

Fig. 5. Accordingly, PPEFs are calm from 13 to 16 October. One needs mark to between 02:00 UT and 04:00 UT on November 10, there is a serious fluctuation and magnetic fluctuation. The other hours of November 10 are magnetically quite calm. While PPEFs appear calm on 27 and 28 November, they display unstable attitudes on 29 November. According to the PPEFs, magnetic oscillation is weak from 1 to 5 December, except 5 December at 21:00 UT. Although slight disturbances are observed magnetically between 6 and 11 December, calmness prevails.

Figure 6 exhibits SA situation by monitoring the F10.7 (sfu) index 61-day discussion period.

The most appropriate index to discuss SA is the zonal index F10.7 (sfu). F10.7 index values above 65–99 sfu for calm SA, 100–150 sfu for moderate SA, and 150 sfu for strong SA should be observed.

Accordingly, while October 12–19, November 11–14, November 20–21, and December 3–11, a quiet and calm SA is observed, a moderate SA is detected between October 20 and November 10, November 15 and 19, and November 22 and December 2.

Examination of the TEC (TECU) map abnormalities

Figure 7 exhibits the oscillation of the TEC data. In this oscillation, one may see the variation of 61 days (61*24 = 1464 h) TEC data.

Presentation of 151 EQ shocks (before the EQ and after the EQ) with $3 \leq M$ that occurred between October 12, 2004, and December 11, 2004, will help to better understand the space weather conditions during the TEC anomaly days. Table 3 displays these 151 EQs. In Table 3, the distribution of 151 EQs that took place in and around the epicenter of the EQ between the dates mentioned and taken from the United States Geological Survey (USGS) is given.

With the help of all these analyses presented above, the study can be concluded by discussing the reasons for the TEC (TECU) anomaly in the ionosphere. It should be noted in this paper that November 11 Alor EQ and November 8 (Dst = −374 nT) super GS occurred in very close time periods (3 days apart). One can examine the day-to-day handling of the TEC anomaly map below:

Anomalies of October 15

Two weak GSs occur on October 13 (Dst = −49 nT) and October 20 (Dst = −32 nT). From October 12 to October 21, space weather conditions are quiet in terms of SA according to Fig. 6. According to PPEFs, there is no condition that may cause the magnetically imbalanced space climate between October 13 and 16. In other words, there are only two weak storms that can cause anomalies in the ionosphere. Although there is a 26-day period between the EQ day and the anomaly day, this date should be noted due to the magnitude of the EQ's severity.

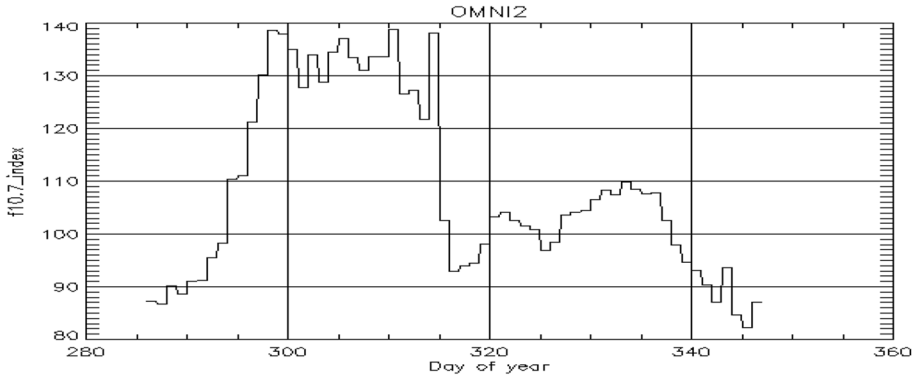

Fig. 6 Attendance of the F10.7 (sfu) index for SA

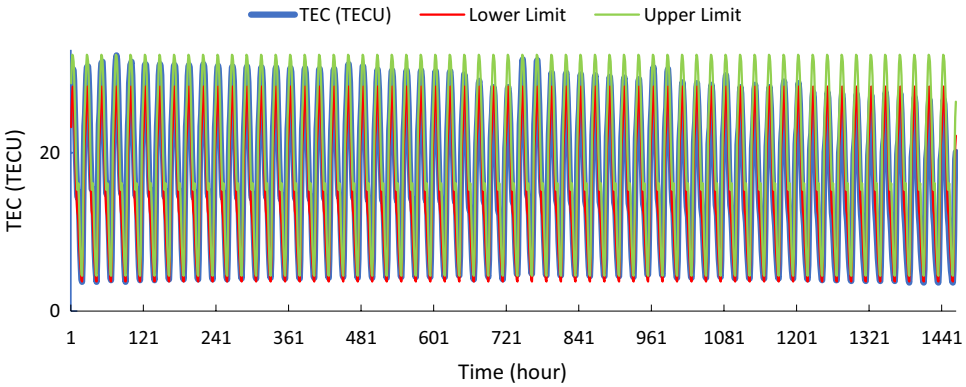

Fig. 7 TEC (TECU) data oscillation for this time domain

Table 3 Earthquakes (EQs) from October 12, 2004, to December 11, 2004

Magnitude	Earthquakes (EQs)								
	$3 \le M < 4$		$4 \le M < 5$		$5 \le M < 6$		$6 \le M < 7$		$7 \le M$
EQ time	Before EQ	After EQ	Before EQ	After EQ	Before EQ	After EQ	Before EQ	After EQ	EQ
Number	1	2	5	121	2	18	–	1	1 (7.5)
	3		126		20		1		1

The source of the October 15 anomaly is likely to be the precursors of the EQ, together with weak GSs.

Anomalies of November 10

November 10 is a very important day because it is the day before the EQ. There is no GS on November 10. But it would be appropriate to look more carefully at the effects of the November 8 superstorm (Dst = --374 nT). The superstorm occurs on November 8 at 06:00 UT. The first CME of this event is observed on November 6, at 15:00 UT. During this ejection, the P (nPa) pressure accelerates from 1.11 nPa to 5.31 nPa, while the N ($1/cm^3$) proton density hits from 5.3 $1/cm^3$ to 18.2 $1/cm^3$. From the first hours of this day, the superstorm tries to move from the main phase to the recovery phase. The variables that make up the storm dynamics tend to calm down and try to return to their pre-storm values. According to PPEFs, a fluctuation is witnessed only between 02:00 UT and 04:00 UT on the 10th of November. Except for these two hours, all hours of the day are magnetically calm. On November 10, the F10.7 index indicates 102.6 sfu. So there is moderate SA that can be called almost calm.

Therefore, the November 10 anomaly observed the day before the EQ is probably caused by the EQ.

Anomalies of December 1–11

The discussion of the anomalies corresponding to these dates should be started by saying that occurred M3 and above 142 aftershocks (Table 3) belong to the Alor EQ. The anomaly table (Table 1), which draws attention to the first 11 days of December, gives clues about aftershocks. First, let us interpret the SA by watching at the behaviors of the

F10.7 (sfu). Accordingly, the F10.7 index indicates moderate SA by showing 107.8 sfu on December 1 and 102.6 sfu on December 2, while staying below 100 sfu on other anomaly days indicates calm SA. Secondly, two weak GSs are detected between these dates. The first one (Dst = −44 nT) of these occurs on December 7, at 02:00 UT, and the other one (Dst = −41 nT) occurs on December 11, at 21:00 UT. Finally, the analysis of these anomaly days can be completed by controlling the magnetic oscillation of the space weather conditions by looking at the PPEFs. Between 1 and 5 December, we encounter a very calm situation magnetically. Only on December 5, between 16:00 UT and 19:00 UT, a short-term magnetic oscillation is observed. While calmness is observed between December 6 and 11, rapid movements (0.3 mV/m) are observed occasionally, which do not need to be noted.

As a result of this December 1–11 anomaly discussion, the source of the December 1–2 anomaly may be moderate SA and aftershocks of the Alor EQ. The source of the December 3–5 anomalies is probably the aftershocks. The source of the anomalies belonging to December 6–11 is probably two weak storms, with the effect of their CMEs, and aftershocks of the EQ.

One of the factors that may cause the anomaly in the ionosphere is volcanoes and the smoke–ash cloud ejected by the volcanoes. In order to steer the volcano discussion, it would be appropriate to examine the 147 large and small volcanoes in the region (https://www.volcanodiscovery.com/indonesia.html) for which activity or restlessness was reported around the earthquake date. In The Dieng volcanic complex, activity was observed in 2005, the closest to the earthquake date. Active Merapi volcano becomes active in 2006, closest to the earthquake date. Lamongan volcano was active in 2003 closest to the earthquake date. In the Raung volcano, activity is observed in the April–October period of 2004. Its activity after this date is July 2005. On May 13, 2004, in the vicinity of the Sirung volcano, although it was written in the local press that this volcano was spewing smoke, it is understood that the news did not reflect the truth. Restlessness is observed at the Ibu volcano between August 2004 and February 2005. This situation is explained by the detection of hot spots in the inner region of the volcano. Therefore, an eruption that can affect the ionosphere is not observed. Awu volcano is one of Indonesia's most dangerous volcanoes. It has been active since the eighteenth century. In June 2004, the eruption of the Awu volcano displaced thousands of people. Soputan volcano erupts on October 18 and December 12. As a result of the explosion, it is observed that the ash-dust cloud is effective. Restlessness is observed on April 13 at Karangetang volcano.

Conclusion

The impact of tectonic movements of the Earth to the ionosphere has been discussed more easily since the 1964 great Alaskan earthquake. Commonly, studies of the ionosphere–earthquake relationship are based on a better understanding of it without rejecting it. Our study supports this relationship, as well. In this study, the investigation of ionospheric anomaly is carried out over the IRI-2016 TEC data. In work, which is handled with the principle of causality and physical facts, the spectrum of amplitudes of the TEC data is checked by Fourier frequency analysis. Then, with the help of the statistical method, hourly anomalies are determined and the daily anomaly list is tabulated. Spectrum analysis and anomaly tables are compatible. Then the reasons for the anomalies are examined in depth. The geomagnetic storm, solar activity, and the earthquake impact are carefully separated from each other to exhibit the space climate conditions. According to these results, the source of the anomaly observed on October 15 is likely two weak storm and the earthquake. The source of the abnormality observed on November 10 is probably the earthquake. The cause of the December 1–2 anomaly may be moderate solar activity and aftershocks. The source of the December 3–5 anomalies is likely the aftershocks. The reason for the anomalies belonging to December 6–11 is likely two weak storms, with the effect of their CMEs, and aftershocks of the earthquake.

Undeniably, the ionospheric anomaly and earthquake relation works have developed in the last years. It is important to show oscillations in the ionosphere in this meaning. Principally, these kinds of studies with the TEC are gradually removing the uncertainties about EQs.

Acknowledgements The author thanks NASA and Kyoto University. The author thanks to the Center for Orbit Determination in Europe (CODE).

Declarations

Conflict of interest The author declares that there are no conflicts of interest.

References

Bagiya MS, Joshi HP, Iyer KN, Aggarwal M, Ravindran S, Pathan BM (2009) TEC variations during low solar activity period (2005–2007) near the equatorial ionospheric anomaly crest region in India. Ann Geophys 27:1047–1057. https://doi.org/10.5194/angeo-27-1047-2009

Baral R, Adhikari B, Calabia A, Shah M, Mishra RK, Silwal A, Bohara S, Manandhar R, Peral LD, Frías MDR (2023) Spectral Features of Forbush Decreases during Geomagnetic Storms. J Atmos Solar Terrest Physi 242:105981. https://doi.org/10.1016/j.jastp.2022.105981

Basciftci F (2021) An analysis of the latest super geomagnetic storm of the 23RD solar cycle (May 15, 2005, Dst: –247 nT). Geomagn Aeron 61:S156–S166. https://doi.org/10.1134/S0016793222010029

Basciftci F (2022) Investigating and comparing the two superstorms in the 23rd solar cycle. Indian J Phys. https://doi.org/10.1007/s12648-022-02396-y

Basciftci F and Bulbul S (2022) Investigation of ionospheric TEC changes potentially related to Seferihisar-Izmir earthquake (30 October 2020, MW 6.6). Bull Geophys Oceanogr. https://doi.org/10.4430/bgo00394

Basciftci F, Bulbul S (2023) Statistical analysis of the regional and global ionosphere model on intense geomagnetic storm. Indian J Phys. https://doi.org/10.1007/s12648-023-02700-4

Basciftci F (2023) Using artificial neural networks in the investigation of four moderate geomagnetic storms (mGSs) that occurred in 2015. Adv Space Res 71(10):4382–4400. https://doi.org/10.1016/j.asr.2023.01.001

Bulbul S and Basciftci F (2021) TEC anomalies observed before and after Sivrice-Elazığ earthquake (24 January 2020, Mw: 6.8). Arab. J. Geosci. 14:1077. https://doi.org/10.1007/s12517-021-07426-3

Bilitza D (2001) International reference ionosphere 2000. Radio Sci 36(2):261–275. https://doi.org/10.1029/2000RS002432

Dautermann T, Calais E, Lognonné P, Mattioli GS (2009) Lithosphere-atmosphere-ionosphere coupling after the 2003 explosive eruption of the Soufriere Hills Volcano, Montserrat. Geophys J Int 179:1537–1546

Davies K, Baker DM (1965) Ionospheric effects observed around time of Alaskan earthquake of March 28 1964. J Geophys Res 70:2251–2253

Dayanandan B, Paul B and Galav P (2020) I. Ionospheric response to the second strongest geomagnetic storm of the solar cycle 24: first results from the Arabian Peninsula. In: 2020 IEEE international conference on wireless for space and extreme environments (WiSEE), Vicenza, Italy, 2020, pp 101–105. https://doi.org/10.1109/WiSEE44079.2020.9262692

Debnath L, Bahatta D (2007) Integral transforms and their applications, second ed., Taylor and Francis LLC.

Eroglu E, Ak N, Koklu K, Ozdemiz Z, Celik N, Eren N (2012) Energy Education Science and Technology Part A: Energy Science and Research 30(1):719–726

Eroglu E (2018) Mathematical modeling of the moderate storm on 28 February 2008. New Astron 60:33–41. https://doi.org/10.1016/j.newast.2017.10.002

Eroglu E (2019) Modeling the super storm in the 24th solar cycle. Earth Planets Space 71(26):1–12. https://doi.org/10.1186/s40623-019-1002-1

Eroglu E (2020) Modeling of 21 July 2017 Geomagnetıc storm. J Eng Technol Appl Sci 5(1):33–49. https://doi.org/10.30931/jetas.680416

Eroglu E (2022a) Discussing total electron content over the solar wind parameters. Math Prob Eng, 2022a, ID 9592008. https://doi.org/10.1155/2022/9592008

Eroglu E (2022b) Ionospheric anomalies related to the Mw 6.5 Samar, Philippines earthquake. Acta Geophys 71(2):601–611. https://doi.org/10.1007/s11600-022-00980-8

Eroglu E (2022c) Ionospheric anomalies related to the Mw 7.1 northern Mid-Atlantic Ridge earthquake. Adv Space Res 71(8): 3382–3393. https://doi.org/10.1016/j.asr.2022.12.010

Eroglu E, Nane E, Goker UD (2023) Seismo-ionospheric anomalies related to the Mw 6.6, July 20, 2017, earthquake in Bodrum, Turkey. Natural Hazards. https://doi.org/10.1007/s11069-023-05914-1

Freund FT, Kulahci IG, Cyr G, Ling J, Winnick M, Tregloan-Reed J, Freund MM (2009) Air ionization at rock surfaces and pre-earthquake signals. J Atmos Sol-Terr Phy 71:1824–1834

Fu HS, Khotyaintsev YV, Vaivads A, Retinò A, André M (2013) Energetic electron acceleration by unsteady magnetic reconnection. Nat Phys 9:426–430. https://doi.org/10.1038/nphys2664

Fu HS, Vaivads A, Khotyaintsev YV, André M, Cao JB, Olshevsky VJ, Eastwood P, Retinò A (2017) Intermittent energy dissipation by turbulent reconnection. Geophys Res Lett 44(1):37–43. https://doi.org/10.1002/2016GL071787

Igarashi G, Saeki S, Takahata N, Sumikawa K et al (1995) Groundwater radon anomaly before the Kobe Earthquake in Japan. Science 269(5220):60–61. https://doi.org/10.1126/science.269.5220.60

Inyurt S, Yildirim O, Mekik C (2017) Comparison between IRI-2012 and GPS-TEC observations over the western Black Sea. Ann Geophys 35(4):817–824

Inyurt S (2020) Modeling and comparison of two geomagnetic storms. Adv Space Res 65(3):966–977. https://doi.org/10.1016/j.asr.2019.11.004

Inyurt S, Razin MRG (2021) Regional application of ANFIS in ionosphere time series prediction at severe solar activity period. Acta Astronaut 179:450–461. https://doi.org/10.1016/j.actaastro.2020.11.027

Isik O, Kocak ZF, Eroglu E (2014) The Investigation of surplus of energy and signal propagation at time-domain waveguide modes. Appl Appl Math Int J (AAM) 9(2):637–645

Ke F, Wang J, Tu M, Wang X, Wang X, Zhao X, Deng J (2018) Enhancing reliability of seismo-ionospheric anomaly detection with the linear correlation between total electron content and the solar activity index F10.7: Nepal earthquake 2015. J Geodyn 121:88–95

Khan AQ, Ghaffar B, Shah M, Ullah I, Júnior JFO, Eldin SM (2022) Possible seismo-ionospheric anomalies associated with the 2016 Mw 6.5 Indonesia earthquake from GPS TEC and Swarm satellites. Front Astron Space Sci Sec Space Phys 9:2022. https://doi.org/10.3389/fspas.2022.1065453

Kim JW, Joo HY, Kim R, Moon JH (2018) Investigation of the relationship between earthquakes and indoor radon concentrations at a building in Gyeongju. Korea Nuclear Eng Technol 50(3):512–518. https://doi.org/10.1016/j.net.2017.12.010

Klotz S, Johnson NL (1983) Encyclopedia of statistical sciences. John Wiley and Sons.

Koklu K (2018) İntegral Dönüşümler ve Uygulamaları, ISBN 978–605–9594–18–9, Papatyabilim Yayınevi, İstanbul, Ocak, 2018 (in Turkish)

Koklu K (2020) Mathematical analysis of the 09 March 2012 intense storm. Adv Space Res 66(4):932. https://doi.org/10.1016/j.asr.2020.04.053

Koklu K (2021) Mathematical analysis of the 08 May 2014 weak storm. Math Probl Eng. https://doi.org/10.1155/2021/9948745

Koklu K (2022) Using artificial neural networks for comparison of the 09 March 2012 intense and 08 May 2014 weak storms. Adv Space Res 70(10):2929–2940. https://doi.org/10.1016/j.asr.2022.07.067

Konakoglu B, Onay FK, Aydemir SB (2023) Tropospheric zenith wet delay prediction with a new hybrid ANN–Gorilla troops optimizer algorithm. Adv Space Res. https://doi.org/10.1016/j.asr.2023.01.035

Lin CC, Shen MH, Chou MY, Chen CH, Yue J, Chen PC, Matsumura M (2017) Concentric traveling ionospheric disturbances triggered by the launch of a SpaceX Falcon 9 rocket. Geophys Res Lett 44:7578–7586

Manoj C, Maus S, Lühr H, Alken P (2008) Penetration characteristics of the interplanetary electric field to the daytime equatorial ionosphere. J Geophys Res 113:A12310. https://doi.org/10.1029/2008JA013381

Manoj C, Maus S (2012) A real-time forecast service for the ionospheric equatorial zonal electric field. Space Weather 10:1–9

Mannucci AJ, Tsurutani BT, Kelley MC, Iijima BA, Komjathy A (2009) Local time dependence of the prompt ionospheric response for the 7, 9, and 10 November 2004 superstorms. J Geophys Res 114:A10308. https://doi.org/10.1029/2009JA014043

Olwendo OJ, Baki P, Cilliers PJ, Mito C, Doherty P (2012) Comparison of GPS TEC measurements with IRI-2007 TEC prediction over the Kenyan region during the descending phase of solar cycle 23. Adv Space Res 49(5):914–921. https://doi.org/10.1016/j.asr.2011.12.007

Ozden Koklu, K. İntegral Denklemler, ISBN 978–605–9594–43–1, Papatyabilim Yayınevi, İstanbul, Mart, 2018 (in Turkish)

Patari A, Paul B, Guha A (2021) Statistics of GPS TEC at the northern EIA crest region of the Indian subcontinent during the solar cycle 24 (2013–2018): comparison with IRI-2016 and IRI-2012 models. Astrophys Space Sci 366:46. https://doi.org/10.1007/s10509-021-03950-6

Paul B, Patari A, De BK, Guha A (2019) Ionospheric irregularities observed during the St. Patrick's Day 2015 severe geomagnetic storm over the southern high latitude polar cap region: a case study from Antarctic Circle. 2019 URSI Asia-Pacific Radio Science Conference (AP-RASC), New Delhi, India, 1. https://doi.org/10.23919/URSIAP-RASC.2019.8738261

Paul B, Gordiyenko G, Galav P (2020) Study of the low and mid-latitude ionospheric response to the geomagnetic storm of 20th December 2015. Astrophys Space Sci 365:174. https://doi.org/10.1007/s10509-020-03884-5

Politis DZ, Potirakis SM, Kundu S, Chowdhury S, Sasmal S, Hayakawa M (2022) Critical dynamics in stratospheric potential energy variations prior to significant (M> 6.7) Earthquakes. Symmetry. 14(9):1939. https://doi.org/10.3390/sym14091939

Satti MS, Ehsan M, Abbas A, Shah M, Júnior JFO, Naqvi NA (2022) Atmospheric and ionospheric precursors associated with Mw ≥ 6.5 earthquakes from multiple satellites. J Atmos Solar Terrest Phys 227:105802. https://doi.org/10.1016/j.jastp.2021.105802

Schaer S (1999) Mapping and predicting the earth's ionosphere using the global positioning system, Ph.D Thesis, Universitat Bern, Switzerland

Shah M, Abbas A, Arqim MA, Ashraf U, Júnior JFO, Tariq MA, Ahmed J, Ehsan M, Ali A (2022) Possible seismo-ionospheric anomalies associated with Mw>5.0 earthquakes during 2000–2020 from GNSS TEC. Adv Space Res 70(1):179–187. https://doi.org/10.1016/j.asr.2022.04.025

Senturk E, Inyurt S, Sertcelik I (2020) Ionospheric anomalies associated with the Mw 7.3 Iran-Iraq border earthquake and a moderate magnetic storm. Ann Geophys 38:1031–1043. https://doi.org/10.5194/angeo-38-1031-2020

Tariq MA, Shah M, Hernández-Pajares M, Iqbal T (2019) Pre-earthquake ionospheric anomalies before three major earthquakes by GPS-TEC and GIM-TEC data during 2015–2017. Adv Space Res 63(7):2088–2099. https://doi.org/10.1016/j.asr.2018.12.028

Tsurutani BT, Gonzalez WD, Gonzalez ALC, Guarnieri FL, Gopalswamy N, Grande M, Kamide Y, Kasahara Y, Lu G, Mann I, McPherron R, Soraas F, Vasyliunas V (2006) Corotating solar wind streams and recurrent geomagnetic activity: a review. J Geophys Res Space Phys 111(A7). https://doi.org/10.1029/2005JA011273

Tsurutani BT, Verkhoglyadova OP, Mannucci AJ, Saito A, Araki T, Yumoto K, Tsuda T, Abdu MA, Sobral JHA, Gonzalez WD, McCreadie H, Lakhina GS, Vasyliūnas VM (2008) Prompt penetration electric fields (PPEFs) and their ionospheric effects during the great magnetic storm of 30–31 October 2003. J Geophys Res 113:A05311. https://doi.org/10.1029/2007JA012879

Yasuoka Y, Ishii T, Tokonami S, Ishikawa T, Narazaki Y, Shinogi M (2005) Radon anomaly related to the 1995 Kobe earthquake in Japan. Int Congr Ser 1276:426–427. https://doi.org/10.1016/j.ics.2004.10.011

Yildirim O, Inyurt S, Mekik C (2016) Review of variations in Mw<7 earthquake motions on position and TEC (Mw=6.5 Aegean Sea earthquake sample). Nat Hazards Earth Syst Sci 16:543–557. https://doi.org/10.5194/nhess-16-543-2016

Springer Nature or its licensor (e.g. a society or other partner) holds exclusive rights to this article under a publishing agreement with the author(s) or other rightsholder(s); author self-archiving of the accepted manuscript version of this article is solely governed by the terms of such publishing agreement and applicable law.